The non-ribosomal peptide synthetase-independent siderophore (NIS) rhizobactin produced by Caballeronia mineralivorans PML1(12) confers the ability to weather minerals

Cintia Blanco Nouche, Cédric Paris, Tiphaine Dhalleine, Philippe Oger, Marie-Pierre Turpault, Stéphane Uroz

TITLE : The Non-ribosomal peptide synthetase-Independent Siderophore (NIS) Rhizobactin produced by *Caballeronia mineralivorans* PML1(12) confers the ability to weather minerals

AUTHORS : Cintia Blanco Nouche[1,2], Cédric Paris[3], Tiphaine Dhalleine[1], Philippe Oger[4], Marie-Pierre Turpault[2], Stéphane Uroz[1,2*]

[1] Université de Lorraine, INRAE, UMR1136 « Interactions Arbres-Microorganismes », F-54000 Nancy, France

[2] INRAE, UR1138 « Biogéochimie des Ecosystèmes Forestiers », F-54280 Champenoux, France

[3] Université de Lorraine, EA 4367 « Laboratoire d'Ingénierie des Biomolécules », Ecole Nationale Supérieure d'Agronomie et des Industries Alimentaires (ENSAIA), F-54505 Vandœuvre-lès-Nancy, France

[4] Université de Lyon, INSA de Lyon, CNRS UMR5240 « Microbiologie, Adaptation et Pathogénie », F-69621, Villeurbanne France

Running title: Rhizobactin, a new NIS involved in mineral weathering

*** Corresponding author:** Mailing address: stephane.uroz@inrae.fr

Université de Lorraine, INRAE, UMR 1136 "Interactions Arbres Microorganismes", F-54000 Nancy, France. Phone: +33 (0)3 83 39 40 81, Fax: +33 (0)3 83 39 40 69.

SUMMARY

To mobilize nutrients entrapped into minerals and rocks, heterotrophic bacteria living in nutrient-poor environments have developed different mechanisms mainly based on acidolysis and chelation. However, the genetic bases of these mechanisms remain unidentified. To fill this gap, we considered the model strain *Caballeronia mineralivorans* PML1(12) known to be effective at weathering. Based on its transcriptomics and proteomics responses in Fe-depleted conditions we pointed a cluster of genes differentially expressed and putatively involved in the production of siderophores. In this study, we report the characterization of this gene region coding for the production of a Non-ribosomal peptide synthetase (NRPS)-Independent Siderophore (NIS). Targeted mutagenesis associated to functional assays and Liquid Chromatography coupled to High-Resolution tandem Mass Spectrometry (LC-HRMS/MS) demonstrated the production of a single siderophore, identified as rhizobactin. This siderophore represents the first NIS containing malic acid in its structure. The evidence of the implication of the rhizobactin in mineral weathering was demonstrated during a hematite dissolution assay. This study provides the first demonstration of the synthesis of a NIS in the genus *Caballeronia* and its involvement in mineral weathering. Our conclusions reinforce the idea that strain PML1(12) is particularly well adapted to nutrient-poor environments.

Keywords: bacteria, mineral weathering, NRPS-independent siderophore, rhizobactin, malic acid

Importance

This work deciphers the molecular and genetic bases used by the strain PML1(12) of *Caballeronia mineralivorans* to mobilize iron and weather minerals. Through the combination of bioinformatics, chemical and phylogenetic analyses we characterized the siderophore produced by strain PML1(12) and the related genes. This siderophore was identified as rhizobactin and classified as a Non-Ribosomal Peptide Synthetase (NRPS)-Independent Siderophore (NIS). Contrary to the previously identified NIS synthetases that form siderophores containing citric acid, α-ketoglutarate, or succinic acid, our analyses revealed that rhizobactin contains malic acid in its structure, representing therefore the first identified NIS with such acid and probably a new NIS category. Last, this work demonstrates for the first time the effectiveness at weathering minerals of a siderophore of the NIS family. Our findings offer relevant information for different fields of research such as environmental genomics, microbiology and chemistry, as well as soil sciences.

INTRODUCTION

Iron represents an essential micronutrient required for living organisms. This element is used as a cofactor by many enzymes and is involved in a wide range of physiological processes such as respiration, DNA synthesis, or photosynthesis [1]. While it is the fourth most abundant element in the Earth crust, it is mainly found under insoluble forms [2,3] in primary (*e.g.,* biotite, granite; Fe^{3+}/Fe^{2+}) and secondary minerals (*e.g.,* hematite, goethite, and magnetite; Fe^{3+}) [4]. In addition, iron is usually poorly bioavailable at neutral to basic pH and under oxygenic conditions. To deal with these limiting conditions and their physiological requirements, bacteria have developed a diversity of mechanisms to mobilize iron and other nutrients poorly available or entrapped into minerals and rocks, a global process termed mineral weathering (MWe).

In heterotrophic bacteria, two main MWe mechanisms have been evidenced: acidolysis and chelation [5]. The first mechanism is related to the action of the by-products of the primary and secondary metabolisms of bacteria. Indeed, by consuming carbon substrates bacteria acidify their local environment due to the production and accumulation of organic acids (*e.g.*, citrate, gluconate) and protons. Such acidification allows the dissolution of the minerals and the release of their nutritive content. The effectiveness of this mechanism is clearly associated to the carbon substrates consumed, with glucose usually giving the stronger acidification [6,7]. The second mechanism is based on the production of chelating compounds such as organic acids (*e.g.,* oxalate) and siderophores. Bacteria can weather minerals using one or both mechanisms (*i.e.*, acidolysis and chelation) depending on the bacterial strain, the nutrient availability, the type of mineral, and the ionic strength of the local environment (*i.e.,* buffering capacity).

Many microorganisms, such as bacteria and fungi, can produce one or more type(s) of siderophore. These particular metabolites are low-molecular weight compounds, characterized

by a strong affinity for iron [8], although they can also chelate other divalent and trivalent cations such as Al, Mg or Cr [9,10]. Siderophores are produced when microorganisms experience nutrient limitation and especially iron deficiency [11]. In this sense, concentrations up to 2 and 12 nM of siderophores have been measured in the solution of nutrient-poor soils [12]. To date, two classes of siderophores have been identified: i) the Non-Ribosomal Peptide Synthetase (NRPS) siderophores (*e.g.*, pyoverdin), and ii) the NRPS-Independent Siderophores (NIS) (*e.g.*, aerobactin) [13]. The contribution of siderophores to MWe has been known for a long time for different types of molecules (*i.e.,* desferrioxamine) in abiotic experiments [14]. However, under such experimental conditions the use of relatively high concentrations of siderophore did not allow to appreciate how microorganisms produced and regulated this production according to their local environment (*i.e.*, pH, ionic strength, nutrient availability) [9,15]. Despite a constant increase in the number of new siderophores identified, their role in MWe has rarely been assessed in a cellular context [6,16,17]. Indeed, few studies have considered how the MWe ability of a mutant impaired in siderophore production compares to that of the wild-type strain and how the nutrient limitations impact the action of the siderophore-mediated weathering.

In this study we have focused on the model strain PML1(12) from the genus *Caballeronia mineralivorans* which has been isolated from a nutrient-poor soil and is known to be effective at MWe and at promoting plant growth [7,18]. However, the molecular basis of its MWe ability is not fully elucidated. The dual transcriptomic and proteomic analyses recently applied on mineral/bacteria interactions highlighted the specific increased expression of a cluster of genes related to iron mobilization and the production of a potential siderophore under Fe depleted conditions [7]. Among these genes the most highly expressed presented high homology with a putative diaminopimelate decarboxylase, cysteine synthase and IucA/IucC synthetase in conditions devoid of iron [7]. In this context, the objectives of this

study were to: i) characterize the cluster of genes conferring the ability to mobilize iron of strain PML1(12); ii) purify and characterize the siderophore produced by strain PML1(12); iii) quantify the contribution of siderophore production on mineral weathering; and iv) study the conservation of the genes involved in siderophore production in the *Burkholderia, Caballeronia, Paraburkholderia* (BCP) group. To do it, different bioinformatic tools were combined to characterize the cluster of genes related to the production of the NRPS-independent Siderophore (NIS) produced by strain PML1(12) and to determine the relative conservation of this cluster of genes in the genome of different strains from the BCP group. The use of a mutant impaired in its ability to produce the siderophore allowed to determine its role in hematite weathering. Ultra-High Performance Liquid Chromatography coupled with High-Resolution Mass Spectrometry allowed the identification of the chelating molecule.

RESULTS

A single genomic region is potentially involved in siderophore production

The CAS assay performed on strain PML1(12) demonstrated its ability to mobilize iron as stated by the formation of a yellow halo around the colony, suggesting the production of one or several siderophores. An antiSMASH analysis of the PML1(12) genome identified a single siderophore production locus. This region is characterized by 10 genes, among which a single gene encoding a protein of 635 amino acids, we named RhiE, presenting the characteristic signature of the *iucA/iucC* domain. Such domain is associated to the synthesis of enzymes involved in the production of NRPS-Independent Siderophores (NIS). The other genes present in the region upstream and downstream of the *rhiE* gene could be involved in siderophore production (*rhiBCD*, intermediate production of the siderophore), transport (*rhiA*, TonB transporter; *rhiF*, MFS transporter; *rhiGHI,* ABC systems) and in the regulation of

siderophore production (*rhiJ)*. The detail of the functions encoded by each gene of the *rhiABCDEFGHIJ* cluster is presented in Table 1.

The rhiABCDEFGHIJ region confers the ability to mobilize iron to strain PML1(12)

To investigate the implication of this region in siderophore biosynthesis, a *rhiE*::Gm knock-out mutant was constructed and tested on solid CAS assay to compare its siderophore production with that of the WT strain (Figure S1). After seven days of incubation, the WT strain presented a yellow halo of *ca.* 1.7 cm, while no halo was visible for the *rhiE*::Gm mutant strain. The lack of production of chelating molecules by the *rhiE*::Gm mutant strain was confirmed with the liquid CAS assay, which showed a very slight $O.D._{655nm}$ decrease from 0.48 ± 0.01 to 0.43 ± 0.01 between the non-inoculated treatment and the *rhiE*::Gm mutant, when the decrease reached a final value of 0.11 ± 0.01 for the WT strain indicative of a trapping of iron from the CAS-Fe(III) complex.

The rhiABCDEFGHIJ cluster permits the growth of strain PML1(12) in iron deficient condition

The growth capabilities of the WT and *rhiE*::Gm strains were measured in a medium devoid of iron (ABm-Fe) amended or not with various concentrations of iron (0, 0.5, 1, 5 and 10 $mg.L^{-1}$ of Fe) (Figure 1). In absence of iron, the growth of the WT strain was delayed and reached a maximum $O.D._{595nm}$ value of 0.58 ± 0.01. The growth rate in absence of iron was significantly lower ($P < 0.05$) than that observed in the presence of iron at 5 or 10 $mg.L^{-1}$ concentration ($O.D._{595nm}$ = 0.88 ± 0.01). The *rhiE*::Gm mutant strain reached the same $O.D._{595nm}$ as the WT strain when growing at the highest iron concentrations (*i.e.*, 5 and 10 $mg.L^{-1}$), but with an important growth delay. The maximal $O.D._{595nm}$ was observed at 50h vs.

163 26h for the *rhiE*::Gm and WT strains, respectively. The largest growth differences (*i.e.*,
164 maximal $O.D._{595nm}$ and delay) between WT and *rhiE*::Gm strains were observed when iron
165 concentrations were below 1 $mg.L^{-1}$ in the solution.
166
167 ***Inhibition of the siderophore production according to Fe concentration***
168 As the production of chelating molecules is usually dependent on Fe concentration in
169 the medium, we assayed the production of siderophores in a range of concentrations of Fe
170 from 0 to 5 $mg.L^{-1}$. After a 3-day incubation period in ABm-Fe amended or not with iron (*i.e.,*
171 $FeCl_3$), the analyses done on the culture supernatant revealed the lack of chelating activity in
172 the non-inoculated controls and in the WT cultures in presence of iron concentrations at 0.8
173 $mg.L^{-1}$ (Figure 2), while this activity was detectable at 0.7 $mg.L^{-1}$ and below. Chelating
174 activity reached its maximum in absence of iron in the medium. The same experiment
175 performed with the *rhiE*::Gm mutant did not reveal any chelating activity whatever the iron
176 concentration tested.
177
178 ***Hematite weathering***
179 The ability of the chelating molecule(s) produced by strain PML1(12) to weather
180 minerals was evaluated considering hematite, an iron-rich mineral, as the sole source of iron
181 in our experimental conditions. To limit the impact of acidification on the mineral weathering
182 process, experiments were done in buffered ABm-Fe medium over 7 days of incubation. The
183 pH of the medium was controlled before and after the experiments in presence/absence of
184 bacterial inoculum and hematite and remained stable (pH = 6.1). In absence of hematite, the
185 WT strain grew in the buffered ABm-Fe medium to an $O.D._{595nm} = 0.47 \pm 0.01$. The presence
186 of hematite in the medium significantly increased growth of the WT strain ($O.D._{595nm} = 0.82 \pm$
187 0.01), while hematite addition had no impact on growth of the *rhiE*::Gm mutant ($O.D._{595nm} =$

188 0.45 ± 0.01 in presence vs. $O.D._{595nm}$ = 0.44 ± 0.02 in absence of the mineral). The CAS assay
189 confirmed that only the WT strain was presenting an active chelating activity in both
190 conditions (*e.g.*, in the presence or in the absence of hematite). Quantification of the iron
191 released in solution from hematite highlighted significantly higher concentrations of iron for
192 the WT strain ([Fe]= 0.76 ± 0.02 $mg.L^{-1}$; $P<0.05$) than for the *rhiE*::Gm mutant (0.04 ± 0.02
193 $mg.L^{-1}$) and the non-inoculated control (0.06 ± 0.02 $mg.L^{-1}$) (Figure 3).
194
195 ***Rhizobactin is the siderophore produced by strain PML1(12)***
196 Pre-purified supernatants from 3-day cultures of *rhiE*::Gm mutant and WT strains
197 were analyzed by HPLC after purification. For this experiment, the growth was performed in
198 ABs-Fe with succinate as sole carbon source to limit the production of exopolysaccharides,
199 which are not compatible with the purification steps. The comparison of the HPLC
200 chromatograms from the WT and *rhiE*::Gm strains as well as from the medium alone
201 highlighted one major difference, a peak (peak #1) with a retention time (RT) of 0.84 min in
202 the WT supernatant. This peak was 2.8 and 3.8 times more intense for the WT strain than for
203 the *rhiE*::Gm mutant strain and the non-inoculated medium, respectively (Figure 4A). To
204 correlate the HPLC chromatograms with the presence of chelating activities, the HPLC
205 fractions were collected and assayed using the CAS assay. The CAS assay was positive for
206 two fractions for the WT samples. The first positive fraction with the CAS assay ($O.D._{655nm}$ =
207 0.06) was collected between 0.77 and 0.97 min corresponding to peak #1 region. The second
208 positive fraction ($O.D._{655nm}$ = 0.14) was identified between 3.74 and 3.95 min. Detailed
209 analysis of the HPLC profiles within this retention time highlighted the presence of a small
210 peak (peak #2), only for WT strain (Figure 4B).
211 To identify the siderophore produced by strain PML1(12), we performed a HPLC-
212 PDA-HRMS/MS analysis of the two fractions mentioned above. High resolution MS analysis

revealed the presence of a single molecule with the same exact mass of 377.1868 Da (monoprotonated ion seen at m/z = 378.1868) in both active fractions and with the theoretical formula $C_{15}H_{25}O_8N_3$ (Figure 5A). Such compound was found only in the WT fractions (and not in the *rhiE*::Gm strain, nor in the negative control). An additional MS signal with m/z = 431.0982 was also specifically observed in the two active WT fractions and was unambiguously attributed to the ferric complex $[(C_{15}H_{25}O_8N_3\text{-}2H) + {}^{56}Fe(III)] + (m/z_{theo} = 377.1788\text{-}2 \times 1.008 + 55.935 = 431.0978$, with $^{56}Fe = 55.935$ u and $^{1}H = 1.008$ u). Indeed, the experimental isotopic pattern was in perfect agreement with the simulated one (Figure 6), thanks to the clear observation of the contribution of ^{54}Fe isotope at m/z = 429.1029 ($[(C_{15}H_{25}O_8N_3\text{-}2H) + {}^{54}Fe(III)]^+$). The previous mass spectrometric observations allow to conclude with certainty that compound of exact mass M = 377.1788 Da can bind iron (III) efficiently and corresponds to the siderophore produced by strain PML1(12).

Such exact mass of 377.1868 Da has been previously associated to the siderophore rhizobactin by Smith *et al.* [19] in a strain of *Ensifer meliloti* and Kügler *et al.* [20] in the strain *Pseudomonas* sp. FEN. In order to elucidate the siderophore highlighted in PML1(12), a tandem mass spectrometry experiment (MS/MS) was performed (Figure 5B). Noticeably, our analyses identified the same four major product ions characterizing the rhizobactin described by Kügler *et al.* [20] (Figure 5C) as : i) m/z = 289.1351 (formed as a result of loss of alanine), ii) m/z = 200.0882 (formed as a result of loss of ethylenediamine and alanine and an additional carboxylic group), iii) m/z = 116.0681 (identified as malic acid ion) and iv) m/z = 84.0790 (identified as decarboxylated lysine ion). Overall, these analyses demonstrate that PML1(12) produces rhizobactin, a siderophore composed of a lysine, an alanine, an ethylenediamine group and malic acid. This work represents the first demonstration that rhizobactin is a NRPS-independent siderophore. Furthermore, it confirms that rhizobactin is

237 based on malic acid and not on other known NIS substrates (citric acid, α-ketoglutarate, or
238 succinic acid).
239
240 ***Comparative genomics of rhizobactin synthesis***
241 A BlastP search of the nr database using the RhiE protein as template allowed the
242 identification of several homologous proteins presenting a percentage of identity ranging from
243 64% to 85% and good sequence coverage (95 to 100%). The best hits appeared assigned to
244 the genera *Paraburkholderia, Trinickia, Vogesella, Polaromonas* or *Pseudomonas*.
245 Noticeably, a homologue was found in strain FEN of *Pseudomonas sp.* (63.5% homologue to
246 RhiE; NCBI accession number WP_191487624.1), a strain described previously for its ability
247 to produce rhizobactin, but in which the synthesis genes had not been identified. Focusing on
248 the *Burkholderiaceae*, we identified 38 proteins presenting a percentage of identity ranging
249 from 34% to 85% and belonging to the genus *Paraburkholderia*, *Trinickia*, *Cupriavidus* and
250 *Ralstonia.* Considering the BCP group, besides the homologues in *Caballeronia*, we found
251 RhiE homologues only in 5 strains assigned to *Paraburkholderia (sp.* BL23I1N, *P.*
252 *haematera, P. sp.* T12-10, *P. sp.* NMBU_R16 and P. *sp*. Ac-20340), organized almost
253 identically as in PML1(12) (*i.e.,* cluster *rhiABCDEFJ*) (Figure 7), but with a variable number
254 of genes. Noticeably, the ABC transport systems were not always present.
255 The phylogenetic analysis of NIS synthetases usually clusters them according to their
256 substrate specificity [13]. To position the RhiE synthetase of strain PML1(12) in the NIS
257 classification and to determine its relatedness to the known NIS synthetases, we constructed a
258 N-J phylogenetic tree of a representative set of known NIS synthetases (Figure 8). A total of
259 24 protein sequences of NIS synthetases which function, and substrate, are known were
260 considered, as well as RhiE protein sequence of PML1(12) and the two homologous RhiE
261 protein sequences identified in *Pseudomonas* FEN and *Ensifer (Sinorhizobium) meliloti* AK83

which are also potentially involved in rhizobactin production. Overall, our results confirm that NIS synthetases are distributed according to their substrate specificity [13,21-23]. The newly characterized RhiE NIS synthetase of strain PML1(12), as well as the two homologues from *Pseudomonas* and *Ensifer*, cluster in group A', forming a well-supported sub-branch within this group. Cluster A' is the only in the phylogeny which does not seem to follow substrate specificity. Indeed, as demonstrated in the current work, RhiE and homologues synthesize rhizobactin, which is based on the use of malic acid as substrate (see above), while others NIS from this cluster use citric acid to synthesize siderophores such as rhizoferrin. The low support of the tree at the base of this cluster (bootstrap values of 37 and 42) may indicate a problem of phylogenetic resolution using the current set of data.

The comparison of the complete genomic region of the cluster of genes involved in rhizobactin transport and production (*rhiABCDEFGHIJ*) (Table 1) found in strain PML1(12) with the genomes of the strains already known to produce rhizobactin (*Ensifer meliloti* and *Pseudomonas* sp. FEN) highlighted a partial conservation of this cluster (*i.e., rhiBCDEF*). The clusters differed however in several instances: i) the presence of a TonB system in the upstream region in strain PML1(12) and at the downstream end in strain AK83 (AEG58212.1) and ii) the absence of two ABC-transport systems (*rhiHI*) and the transcriptional regulator (*rhiJ*) in strains AK83 and FEN (Figure 7).

DISCUSSION

Rhizobactin identification

Rhizobactin was first described in the plant-associated bacterial strain *Ensifer meliloti* DM4 (former *Sinorhizobium meliloti*) [19]. This first study provided a detailed chemical composition based on mass spectrometry and NMR analyses, revealing that this carboxylate siderophore was formed by an ethylenediamine group coupled with alanine, lysine, and malic

287 acid. The same siderophore was reported more recently for a bacterial strain isolated from a
288 nutrient-poor environment, the strain *Pseudomonas sp.* FEN [20]. Both studies provided the
289 chemical characterization of this molecule, but neither the genetic characterization nor the
290 classification of rhizobactin. Interestingly, *Pseudomonas sp.* FEN can produce rhizobactin and
291 rhizobactin B, rhizobactin B being the main siderophore produced. Structurally, these two
292 siderophores differ only by the presence of a methyl group at the C2 position of malic acid,
293 giving a citramalic acid in rhizobactin B instead of a malic acid in rhizobactin. A third
294 rhizobactin type was identified in strain 1021 of *Ensifer meliloti* (*i.e.,* rhizobactin 1021), but
295 completely different in terms of chemical structure from the one described above. This
296 hydroxamate siderophore of 530 Da is based on a citrate derivative with the carboxyl groups
297 linked to two different side chains [23]. In our study, we identified the siderophore produced
298 by strain PML1(12) using a combination of CAS assay, HPLC purification and MS/MS
299 analyses. This molecule not only binds the different iron isotopes but also presented an exact
300 mass (377.1868 Da) and a fragmentation pattern like that of the rhizobactin identified in
301 *Ensifer meliloti* strain DM4 and *Pseudomonas sp.* strain FEN [19,20]. Our *rhiE*::Gm mutant
302 of strain PML1(12), which is unable to chelate iron, proves the involvement of the *rhiE* gene
303 cluster in the production of the unique siderophore molecule produced by strain PML1(12).
304 Noticeably, the rhizobactin gene cluster appeared relatively conserved in the two strains
305 already described for the production of rhizobactin, though the strain *Pseudomonas sp.* FEN
306 presented an additional gene identified as a citrate lyase (WP_191487621.1), which is the first
307 gene of the cluster in this strain, upstream of the *rhiE* homologue. Citrate lyase, may be
308 involved in the process of transformation of malic acid into citramalic acid, explaining why
309 rhizobactin B is the main siderophore produced by strain *Pseudomonas sp.* FEN, while
310 rhizobactin is produced by *Ensifer meliloti* AK83 and strain PML1(12).
311

Rhizobactin as NRPS-Independent Siderophore

Two groups of bacterial siderophores are currently described according to their biosynthetic pathway. The first pathway uses complex, modular, multidomain enzymes known as NRPS [6,13,24]. The second relies on NRPS-independent synthetases [13,25]. In comparison to the wealth of information available on the genetics and chemistry of the NRPS siderophores, NIS and their related biosynthetic pathways are still poorly documented [25]. This is an important point because siderophores cannot be categorized as NIS or NRPS without a proper genetic characterization. In this sense, rhizobactin was discovered and chemically characterized by Smith *et al*. [19], as early as 1984, in strain *Ensifer meliloti* DM4, but could only be classified as a NIS thanks to the current study and its homology at chemical ($C_{15}H_{25}O_8N_3$) and genomic level (gene cluster) to that of strain PML1(12). The strain PML1(12) presents a gene cluster of 10 genes (Figure 7) with the characteristic signature of the NIS synthesis pathway as identified for the first described NIS (*i.e*., aerobactin) [26, 27]. The aerobactin-synthetases, *iucA* and *iucC* became since that, the hallmarks of the presence of NIS in genomes [22], either in a single copy such as for the synthesis of rhizoferrin (*e.g.,* FslA) in *Francisella tularensis* [28] or rhizobactin in strain PML1(12) (*e.g*., RhiE, this study) or either in several copies such as for the synthesis of aerobactin (*e.g.,* IucA and IucC) [27]. Our findings will enrich the NIS database and improve the siderophore determination using AntiSMASH.

Rhizobactin a new class of NIS?

NIS synthetases traditionally separate in five phylogenetic groups (A, A', B, C and C'). This classification which was obtained on experimentally demonstrated NIS synthetases is congruent with their substrate specificity with: i) type A and A' specific for citric acid; ii) type B for α-ketoglutarate intermediates; and iii) type C and C' specific for citryl or succinyl-

based intermediates [13]. The number of experimentally demonstrated NIS synthetases is limited and consequently their position in phylogenetic trees may change with the evolution of NIS studies. As an example, the SfaB and SfaD enzymes responsible for the synthesis of Staphyloferrin A which presents a citric acid in its structure [29] were initially included in group B, a group of NIS synthetases specific for α-ketoglutarate. With the discovery of other novel citric acid-based and chiral siderophores (*e.g.*, rhizoferrin, legiobactin) SfaB and SfaD now cluster within a new group, named A'. Our phylogenetic tree agrees with those previously published [13,21,22], confirming that the NIS synthetases mostly cluster according to their substrate specificity. In this respect, the rhizobactin synthetase clusters with group A', which corresponds to citrate-based and chiral siderophores. However, rhizobactin and rhizobactin B synthetases form a well-supported branch within group A'. Malic acid (rhizobactin) and citramalic acid (rhizobactin B) have never been described previously as possible substrates for NIS synthetases. Therefore, the difference of substrate specificity between rhizobactin synthetases (malic for rhizobactin and citramalic acid for rhizobactin B) and synthetases from group A' (citric acid), and the absence of other already characterized synthetases with malic acid as substrate, allow us to propose a new group of NIS called D. The future characterization of new NIS synthetases that use malic/citramalic acid as substrate should make more robust the separation from A' group, as it happened previously for groups B and A' [29].

Role of rhizobactin in mineral weathering

Iron is considered as an essential element and its deficiency alters the growth of bacteria [6,30,31]. Strain PML1(12) follows this rule, with a strong delay and decrease in growth in iron deprived conditions compared to non-limiting conditions. To adapt to low-iron conditions, bacteria can produce siderophores, whose production is regulated by the quantity

of iron available and stopped at a maximum of 5 $mg.L^{-1}$ of Fe [32]. Here, we showed that the production of rhizobactin by strain PML1(12) was detectable until an iron concentration of 0.7 $mg.L^{-1}$. Such iron regulation fits with the observations done by the dual transcriptomic and proteomic analyses on strain PML1(12) in the presence/absence of a mineral carrying iron (*i.e.,* biotite), which evidenced that the genes involved in siderophore production were only up-regulated in Fe-depleted conditions and in the absence of mineral [7]. Although minerals represent an important source of iron, the production of siderophores remains strongly determined by the iron bioavailability and the local conditions (pH, ionic strength). Several studies have demonstrated that in oligotrophic conditions minerals may be seen as a source of iron if siderophore-producing bacteria are present in the environment [33]. The effectiveness of siderophores at solubilizing iron from different minerals is known and demonstrated for a long time in abiotic conditions. As an example, desferrioxamine B was proved to weather Fe from several iron oxides [15]. Even more, rhizoferrin and desferrioxamine A and B are not only effective at mobilizing Fe from hydroxide minerals, but also other metals such as chromium [34,35]. However, such abiotic experiments were usually based on high concentrations of siderophores and did not permit to consider all the regulation occurring in bacteria according to nutrient availability, ionic strength of the medium and mineral type. In contrast, few studies investigated the ability of siderophore-producing bacteria to liberate nutrients trapped in minerals in a cellular context, considering mutants impaired in their ability to produce siderophores. Our study represents the first demonstration of the role of a NIS (*i.e.*, rhizobactin) produced in biotic conditions in the weathering of hematite. Such demonstration completes the list of siderophores already characterized for their role in mineral weathering [6,16,17,33].

Occurrence of the Rhizobactin siderophore in the BCP group

Among members of the same genus or species, the type of siderophore produced can strongly differ (*i.e.*, rhizoferrin biosynthesis) [36,37] or on the contrary be very conserved (*i.e.,* pyoverdine biosynthesis)[38]. Members of the *Burkholderia sensu lato* are well known for the different strategies they use to mobilize iron based on siderophore-independent (Ftr) [39] and siderophore-dependent (*e.g.,* ornibactin) [40,41] systems, but not yet based on a NIS. Our study represents the first evidence of the production of rhizobactin in this group. Based on this evidence, we evaluated the distribution of a homologue of the *Caballeronia mineralivorans* strain PML1(12) RhiE NIS synthetase and the conservation of the *rhi* cluster of genes. Our analysis revealed that homologues of RhiE can be found in many genera among Beta-proteobacteria, but the most represented remains the *Pseudomonas* genus. In this context, *Pseudomonas sp.* FEN is the only strain characterized for its ability to produce rhizobactin, while many *Pseudomonas* strains have been described for their ability to produce NRPS siderophores (*e.g.,* pyoverdin) [38]. Focusing on the BCP group (including *Burkholderia, Paraburkholderia* and *Caballeronia*), only five *Paraburkholderia* strains (*P.* sp. BL23I1N, *P. haematera,* sp. T12-10, *P.* sp. NMBU_R16 and *P.* sp. Ac-20340) presented the rhizobactin cluster, questioning its origin. In terms of ecology, many of the strains we identified to possess a rhizobactin synthesis locus homologue originate from the rhizosphere (*e.g., Paraburkholderia sp.* T12-10, R16 and Ac-20340 and most of the members of *Trinickia, Vogesella, Polaromonas* or *Pseudomonas*) and nutrient-poor ecosystems suggesting a role in plant nutrition and adaptation to nutrient-poor conditions. The role of siderophore-producing bacteria in plant nutrition and growth promotion has already been demonstrated as in the case of the strains *Burkholderia pyrrocinia* JK-SH007 [40] or *Caballeronia mineralivorans* PML1(12) [42,43].

Conclusion

412 It is clearer and clearer that the ability of bacteria to weather minerals is finely
413 regulated by local conditions and physiological processes. Nutrient availability, ionic strength
414 of the medium and the type of mineral and of the carbon substrate metabolized, strongly
415 determine the mechanism used by bacteria and the effectiveness at weathering. While the
416 global mechanisms are identified (*i.e.*, acidification, chelation, oxido-reduction), the genetic
417 and geochemical bases remain poorly documented. Demonstrations in a cellular context (*i.e.*,
418 effect of a gene mutation) are essential to cover without *a priori* the diversity of mechanisms
419 used by phylogenetically different bacteria and to decipher the regulations of these
420 mechanisms occurring according to the mineral type and the local conditions. The
421 combination of molecular and (geo-)chemical techniques used here not only allowed the
422 identification of the siderophore produced by strain *Caballeronia mineralivorans* PML1(12)
423 as rhizobactin, but also its classification as an NRPS-independent siderophore (NIS) and its
424 contribution to mineral weathering. Our study provides new information regarding the
425 complexity of mechanisms used by this model strain according to the local conditions and its
426 metabolism. Our results highlight that siderophores play an essential role in mineral
427 weathering under buffered and non-acidifying conditions, while organic acid and proton-
428 based mechanisms represent the main mineral weathering mechanism used by this strain
429 under non-buffered and acidifying conditions. The ability of rhizobactin to weather more
430 complex and less weatherable minerals, with a lower iron content (*e.g.,* biotite) remains to be
431 determined. Together, our results clearly highlight how the strain PML1(12) is well adapted
432 to live in nutrient-poor environments and to develop complex and finely regulated
433 mechanisms to mobilize nutrients from minerals.
434
435 **MATERIALS AND METHODS**
436 **Bacterial strains and growth media**

Bacterial strains and plasmid are listed in Table 2. The model *Caballeronia mineralivorans* strain PML1(12) was isolated from the ectomycorrhizosphere of *Scleroderma citrinum* associated with oak (for sampling details see Calvaruso *et al*. [44])

Strains, with the exception of *Escherichia coli*, were grown in AB medium [45] supplemented with mannitol (ABm) or succinic acid (ABs) (2 $g.L^{-1}$ final concentration) at 25 °C. A version of the AB medium devoid of iron was also used (AB-Fe). *E. coli* strains were grown in Luria-Bertani (LB) at 37 °C. When required, gentamycin, kanamycin and ampicillin were added to the media at a final concentration of 20, 50 and 100 $\mu g.mL^{-1}$, respectively.

Preparation of bacterial inoculum of Caballeronia mineralivorans strain PML1(12) and its mutant

For each of the assays presented in this work, the wild-type (WT) strain and the *rhiE*::Gm mutant strain were recovered from glycerol stock (-80 °C) and grown on solid ABm medium (25 °C) for 2 days. One isolated colony of each strain was inoculated in 10 mL of liquid ABm medium and incubated 3 days at 25 °C under 150 rpm agitation. Liquid cultures were centrifugated at 9000 g for 15 min at 4 °C and the pellet was washed three times with sterile MilliQ water. The pellet was resuspended in sterile MilliQ water, and the optical density was adjusted to $O.D._{595nm} = 0.9 \pm 0.03$ (corresponding to 2.10^9 cell/mL).

rhiE::Gm mutant construction

Total DNA was extracted from the WT strain PML1(12) using the protocol of Pospiech and Neumann [46]. To construct a targeted mutant of the gene homologous to *iucA/iucC* (*rhiE*), the total gene was amplified using a combination of primers including For-*rhiE* and Rev-*rhiE* for a complete amplification and Rev-*rhiE_Sma*I and For-*rhiE_Sma*I to insert a *Sma*I site (Table 2; Figure S2 for details). The insertion of a *Sma*I site in the middle of

462 the *rhiE* gene was done following 3 PCR rounds: i) For-*rhiE* with Rev-*rhiE_Sma*I (967 bp),
463 ii) For-*rhiE_Sma*I with Rev-*rhiE* (966 bp) and iii) For-*rhiE* and Rev-*rhiE* (1908 bp). The PCR
464 products of PCR1 and 2 were purified and used as matrix for PCR 3. After amplification and
465 purification, PCR3 product was ligated into the pGEM-T Easy plasmid (Promega) resulting in
466 the plasmid pGEM-*rhiE_Sma*I (Table 2). The plasmid pGEM-*rhiE_Sma*I was then digested
467 with *Sma*I to introduce the *Sma*I-digested gentamycin (Gm) resistance cassette from plasmid
468 pUC1318, resulting in the plasmid pGEM-*rhiE*::Gm. A fragment containing the *rhiE*::Gm
469 cassette was then obtained by *Eco*RI restriction and cloned in the plasmid pK19mob, resulting
470 in the pK19mob-*rhiE*::Gm plasmid. This construction was transferred to *E. coli* S17.1λpir and
471 then to strain PML1(12) by bi-parental conjugation. Δ*rhiE* mutants were recovered after 5
472 days of incubation at 25 °C on gentamycin-containing ABm plates. The transconjugants
473 obtained were verified by PCR with For-*rhiE* and Rev-*rhiE* primers, to differentiate the single
474 and double cross-over events. Several single and double-cross-over mutants were obtained
475 and conserved. The experiments described in our study were done using a double cross-over
476 mutant named *rhiE*::Gm.
477
478 **Siderophore activity**
479 Siderophore activity was detected using the liquid and solid versions of the Chrome
480 Azurol S (CAS) assay according to Schwyn and Neilands [47]. For both assays, the color
481 change, sign of the chelating activity of the siderophore for the iron (III) of the CAS-Fe
482 complex can be quantified by the presence of a halo on the solid CAS assay or through the
483 measurement of the optical density (O.D.) at 655 nm for the liquid assay.
484 For the solid CAS assay, 5 µL of the bacterial inoculum (both WT and mutant strains;
485 corresponding to 5.10^6 colonies forming unit (CFU)) were inoculated in triplicate in agar

plates and incubated three days at 25 °C. The diameter of colony and the halo surrounding it were measured to determine growth and siderophore(s) production, respectively.

For the liquid CAS assay, 0.5 mL of the bacterial inoculum (both WT and mutant strains; corresponding to 5.10^8 CFU) were inoculated in triplicate in 4.5 mL ABm-Fe. After 3-days incubation at 25 °C under agitation (150 rpm), the cultures were centrifugated at 9000 g during 15 min at 4 °C to recover culture supernatants. A volume of 100 µL of these supernatants were mixed with 100 µL of CAS-Fe(III) and incubated during 1h at room temperature in the dark. Then, the O.D. was measured at 655 nm using a microplate reader (Bio-Rad, model iMark). Decrease of absorbance at this specific wavelength is synonym of siderophore presence (change of media coloration from blue to yellow [6, 47]). Non-inoculated medium was used as negative control for the liquid assay.

Impact of iron concentration on the growth the WT and *rhiE*::Gm strains

To determine if the concentration of iron and the mutation of the *rhiE* gene (*rhiE*::Gm mutant) affected the growth of strain PML1(12), growth was determined at different iron concentrations (*i.e.,* 0, 0.5, 1, 5, 10 $mg.L^{-1}$ of Fe). A bacterial inoculum of 10 µL (corresponding to 6.10^6 CFU) was added to 190 µL of ABm-Fe and incubated in 96-well microplates for 5 days. This experience was performed in triplicate and conducted at 25 °C on orbital shaking in a microplate reader (Tecan infinite M200 pro). The absorbance was measured at 595 nm every 3 hours. To evaluate the growth of the strains, the slope of the exponential phase (*i.e.*, growth rate) was calculated for each condition and replicate.

Siderophore production inhibition

Siderophore production is known to be regulated by the availability of nutritive elements in the culture medium, especially iron. To evaluate the concentration of Fe necessary

511 to inhibit the siderophore production, the WT and mutant strains were incubated at different
512 iron concentrations. Non-inoculated conditions were used as negative controls for each
513 concentration. A volume of 10 µL of inoculum was added to 180 µL of ABm-Fe
514 supplemented with 10 µL of different $FeCl_3$ stock solutions ranging from 0 to 5 $mg.L^{-1}$ of Fe
515 to obtain the following final concentrations in the medium: 0, 0.1, 0.2, 0.3, 0.4, 0.5, 0.6, 0.7,
516 0.8, 0.9, 1, 1.5, 2, 2.5, 5 $mg.L^{-1}$. The 96-well microplates were incubated 3 days at 25 °C.
517 Then, microplates were centrifugated at 3000 g during 15 minutes at 4 °C and 100 µL of
518 supernatant were mixed with 100 µL of CAS-Fe(III). After 1 h incubation in the dark the
519 plates were read at 655 nm using a microplate reader (Bio-Rad, model iMark) as described
520 above.
521
522 **Hematite weathering assay**
523 *Hematite characteristics*
524 Hematite (Fe_2O_3) is an iron-oxide mineral widely distributed in all soils [48] and
525 characterized by a high iron content. The hematite used in this study comes from a batch
526 extracted in Brazil. The chemical composition was determined on crushed powder by
527 inductively coupled plasma-atomic emission spectrometry (700 Series ICP-AES, Agilent
528 Technologies) as described in Picard *et al.* [49]. This analysis revealed that the hematite used
529 is mainly composed of Fe_2O_3 (99.3%) and also contains in small amounts: 0.40% TiO_2, 0.18%
530 SiO_2, 0.16% Al_2O_3, 0.10% MgO, 0.037% MnO.
531
532 *Mineral weathering assay*
533 To avoid contamination by residues associated with glass tubes, all glassware was
534 rinsed once with 3.6% HCl and then three times with MilliQ water. The tubes were filled with
535 200 mg of hematite and 9 mL of ABm-Fe medium and autoclaved at 121 °C. To evaluate the

differences in the weathering ability of the *rhiE*::Gm mutant and the WT strains, 1 mL of each inoculum was added to the tubes (procedure performed in triplicate). Non-inoculated media with and without hematite were used as abiotic and sterility controls for weathering. Samples were incubated for 7 days under agitation at 150 rpm and 25 °C.

The cultures were used to determine: i) bacterial growth, ii) solution pH, iii) siderophore production and iv) iron concentrations. Bacterial growth was estimated directly on the liquid culture by measuring the $O.D._{595nm}$ on 200 µL. The other measurements were done after centrifugation at 14000 g for 15 min to remove bacterial cells and hematite particles. A volume of 100 µL of supernatant was used to evaluate the level of siderophore(s) production using the liquid CAS assay according to the protocol described above. A volume of 180 µL of supernatant was used to measure the pH by mixing with 20 µL of bromocresol green (1 $g.L^{-1}$) according to [18]. For the measure of the iron concentration, the supernatant was filtered at 0.22 µm (GHP Acrodisc 25 mm syringe filter; PALL) before mixing 180 µL of supernatant with 20 µL of ferrospectral. Both pH and iron determinations are based on optical density measurements at 595 nm using a microplate reader (Bio-Rad, model iMark) and after conversion with the calibration curves done on the bromocresol green and ferrospectral dyes, according to [18].

Chemical characterization of the siderophore

Siderophore production and purification

Volumes of 50 mL of ABs-Fe were inoculated with each strain (WT and *rhiE*::Gm) and incubated at 25 °C under 150 rpm shaking for three days. Succinic acid was used here as sole carbon source to limit the production of exopolysaccharides. A non-inoculated condition was also included as negative control. After the incubation time, cultures were centrifugated at 9000 g, during 15 min at 4 °C. The supernatant was filtered using 0.45 µm filters

561 (Millipore) and treated with a Sep pack Vac 6cc tC18 Cartridge (Waters) to pre-purify and
562 concentrate the siderophore(s). The columns were first washed with 10 mL of 100% ethanol
563 and then equilibrated with 10 mL of 0.01% trifluoroacetic acid (TFA). After this equilibration
564 step, a volume of 25 mL of supernatant was added progressively to the column and finally the
565 different fractions of the supernatant were eluted by the addition of 5 mL of 10% and then
566 20% methanol in water. At each step the eluted volume (*ca.* 5 mL) was recovered and
567 concentrated in the SpeedVac system. The dried samples were resuspended in 100 µL of
568 MilliQ water. These pre-purified fractions were used for further characterization using the
569 liquid CAS assay to verify the presence of siderophore.
570
571 *High Performance Liquid Chromatography (HPLC) analyses and fractionation*
572 The different pre-purified fractions recovered above (from WT, mutant and negative
573 control samples) were analyzed by HPLC. A volume of 50 µL of each extract was injected in
574 a Gemini C18 column (150 x 3.0 mm, 5 µm particle size, Phenomenex). Solvent A consisted
575 of MilliQ water and solvent B consisted of acetonitrile plus 0.2% of TFA. A linear gradient
576 elution from 2% to 40% of solvent B over 25 min at a flow rate of 1 $mL.min^{-1}$ was used to
577 separate compounds. Absorbance was monitored at 210 nm.
578 Peaks of potential interest were identified by comparing the chromatogram of the WT
579 sample with that of the *rhiE*::Gm mutant sample and the negative control. To determine the
580 presence of the siderophore(s) activity, a fraction collection was performed in 96-wells
581 microplates using a fraction collector system (FRC-10A fraction collector system, Shimadzu).
582 Fractions of 200 µL were recovered each 0.2 s using the same HPLC conditions as described
583 before. Fraction collection was performed three times independently, and fractions with the
584 same retention times were pooled. The fractions collected were then concentrated using the
585 SpeedVac and resuspended in 100 µL of MilliQ water. To determine the presence of

586 siderophore(s) activity, a volume of 25 µL of the collected fractions was mixed with 25 µL of
587 liquid CAS and the absorbance at 655 nm was measured after overnight incubation.
588
589 *Qualitative HPLC-DAD-MS-MS/MS analysis of siderophores and ferrosiderophores*
590 A Thermo Scientific UHPLC-HRMS/MS system composed of a Vanquish™ liquid
591 chromatography unit coupled to a photodiode array detector (PDA) and an Orbitrap ID-X™
592 Tribrid™ high-resolution mass spectrometer operating in electrospray ionisation mode (ESI)
593 was used to detect and identify the putative siderophores. Ten microliters of each bacterial
594 extract were injected onto a Hichrom Alltima C18 column (150×2.1 mm - 5 µm) maintained
595 at 25 °C. The flow rate was set at 0.2 $mL.min^{-1}$ and mobile phases consisted in water modified
596 with formic acid (0.1%) for A and acetonitrile modified with formic acid (0.1%) for B.
597 Compounds of interest were eluted using a linear gradient from 5% to 20% of B for 10 min,
598 then a 5 min isocratic step was applied at 98% of B to wash the column, before returning to
599 the initial composition of 5% B for 6 min to reach the equilibrium. Mass analysis was carried
600 out in ESI positive ion mode (ESI^+) and mass spectrometry conditions were as follows: spray
601 voltage was set at 3.5 kV; source gases were set (in arbitrary $units.min^{-1}$) for sheath gas,
602 auxiliary gas and sweep gas at 35, 7 and 10, respectively; vaporizer and ion transfer tube
603 temperatures were both set at 300 °C. Survey scans of precursors were performed from 150 to
604 2000 m/z at 60 K resolution (FWHM at 200 m/z) with MS parameters as follows: RF-lens,
605 35%; maximum injection time, 50 ms; data type, profile; internal mass calibration EASY-IC
606 TM activated; normalized AGC target: 25%. A top speed data dependent MS^2 (0.6 sec for the
607 whole cycle time) was carried out using a wide quadrupole isolation (1.5 Th), a HCD
608 fragmentation with a stepped collision energy (20, 35 and 50%) and an Orbitrap measure at
609 15 K resolution (high-resolution MS/MS analysis). Precursors with an intensity upper than
610 2.10^4 were automatically sampled for MS^2. Dynamic exclusion was used, and the time of

exclusion was set at 2.5 s, with a 10 ppm tolerance around the selected precursor (isotopes excluded). Other MS^2 parameters were as follows: data type, profile; normalized AGC target: 20%; AGC target, 10000.

Mass spectrometer calibration was performed by using the Thermo Scientific Pierce TM FlexMix TM calibration solution. MS data acquisition was carried out by using the Xcalibur v. 3.0 software (Thermo Scientific).

Bioinformatic analyses

Genome analysis

Genome analysis was performed using MicroScope MaGe (Magnifying Genomes) [50] and NCBI. The presence of *iucA/iucC* gene homologue was identified by antiSMASH [51] and confirmed by BLASTP analyses based on sequence homology [52].

Phylogenetic analyses

A total of 27 protein sequences (Table S1) homologous to IucA/IucC, including the homologue of PML1(12) (RhiE), were recovered from NCBI to build a phylogenetic Neighbor-Joining (N-J) tree using the Seaview platform (version 5.0.4)[53]. For this analysis, the protein sequences considered were: i) sequences which role in siderophore biosynthesis were experimentally demonstrated; ii) sequences based on their homology with the RhiE protein identified in strain PML1(12). Protein sequences were aligned using MUSCLE algorithm and then a N-J tree with 100.000 iterations was constructed.

Statistical analyses.

Statistical analyses were performed in R software (Tidyverse packages)[54]. Triplicate samples were used in all experiments. Differences between samples means (pH, growth, CAS assay and released iron) or growth slopes were analyzed by ANOVA and TukeyHSD tests.

Acknowledgements

This work was supported by grants from the EC2CO program of the CNRS and the Labex ARBRE from the French National Research Agency (ANR) to S. U. The UMR1136 and UR1138 are supported by the ANR through the Labex Arbre (ANR-11-LABX-0002-01). C. B.N. is supported by a PhD fellowship from the INRAE and Grand Est Region. The authors thank the MICROSCOPE team (David Roche; Genoscope) for the support provided on the genome management and the SILVATech platform for technical support. The authors also thank the PASM platform for the use of the Orbitrap LC-MS system (Plateau d'Analyse Structurale et Métabolomique - SF4242 EFABA, F-54505 Vandœuvre-lès-Nancy, France).

References

1. Andrews SC, Robinson AK, Rodríguez-Quiñones F. 2003. Bacterial iron homeostasis. *FEMS Microbiol Ecol* 27: 215-237.
2. Desai A, Archana G. 2011. Role of Siderophores in Crop Improvement. *Bacteria in Agrobiology: Plant Nutrient Management* 109–139.
3. Radzki W, Gutierrez Mañero FJ, Algar E, Lucas García JA, García-Villaraco A, Ramos Solano B. 2013. Bacterial siderophores efficiently provide iron to iron-starved tomato plants in hydroponics culture. *ALJMAO* 104: 321–330.
4. Colombo C, Palumbo G, He JZ, Pinton R, Cesco S. 2014. Review on iron availability in soil: interaction of Fe minerals, plants, and microbes. *J Soils Sediments* 14: 538–548.

5. Uroz S, Picard P, Turpault MP. 2022. Recent progress in understanding the ecology and molecular genetics of soil mineral weathering bacteria, *Trends Microbiol* 30: 882-897.
6. Picard L, Paris C, Dhalleine T, Morin E, Oger P, Turpault MP, Uroz S. 2022. The mineral weathering ability of *Collimonas pratensis* PMB3(1) involves a Malleobactin-mediated iron acquisition system. *Environ Microbiol* 24: 784-802.
7. Uroz S, Picard L, Turpault MP, Auer L, Armengaud J, Oger P. 2020. Dual transcriptomics and proteomics analyses of the early stage of interaction between *Caballeronia mineralivorans* PML1(12) and mineral. *Environ Microbiol* 22: 3838-3862.
8. Neilands JB. 1995. Siderophores: structure and function of microbial iron transport compounds. *J Biol Chem* 270: 26723-26726.
9. Kraemer SM, Duckworth OW, Harrington JM, Schenkeveld WDC. 2015. Metallophores and Trace Metal Biogeochemistry. *Aquat Geochem* 21:159–195
10. Shiny Matilda C, Mannully ST, Rao VP, Shanti C. 2021. Chromium binding *Bacillus cereus* VITSH1 - a promising candidate for heavy metal clean up. *Lett Appl Microbiol* 72: 517-525.
11. Kramer J, Özkaya Ö, Kümmerli R. 2020. Bacterial siderophores in community and host interactions. *Nat Rev Microbio* 18: 152-163.
12. Essén SA, Bylund D, Holmström SJ, Moberg M, Lundström US. 2006. Quantification of hydroxamate siderophores in soil solutions of podzolic soil profiles in Sweden. *Biometals* 19: 269-282.
13. Carroll, C.S. and Moore, M.M. (2018). Ironing out siderophore biosynthesis: a review of non-ribosomal peptide synthetase (NRPS)-independent siderophore synthetases. *Crit Rev Biochem Mol Biol* 53: 4, 356-381

14. Torres MA, Dong S, Nealson KH, West AJ 2019. The kinetics of siderophore-mediated olivine dissolution. *Geobiol* 17: 401-416.
15. Cheah SF, Kraemer SM, Cervini-Silva J, Sposito G. 2003. Steady-state dissolution kinetics of goethite in the presence of desferrioxamine B and oxalate ligands: Implications for the microbial acquisition of iron. *Chem Geol* 198: 63–75.
16. Dehner CA, Awaya JD, Maurice PA, DuBois JL. 2010. Roles of siderophores, oxalate, and ascorbate in mobilization of iron from hematite by the aerobic bacterium *Pseudomonas mendocina*. *Appl Environ Microbiol* 76: 2041–2048.
17. Parrello D, Zegeye A, Mustin C, Billard P. 2016. Siderophore-Mediated Iron Dissolution from Nontronites Is Controlled by Mineral Cristallochemistry. *Front Microbiol* 7: 423.
18. Uroz S, Calvaruso C, Turpault MP, Pierrat JC, Mustin C, Frey-Klett P. 2007. Effect of the Mycorrhizosphere on the Genotypic and Metabolic Diversity of the Bacterial Communities Involved in Mineral Weathering in a Forest Soil. *Appl Environ Microbiol* 73: 3019–3027.
19. Smith MJ, Shoolery JN, Schwyn B, Holden I, Neilands JB. 1985. Rhizobactin, a structurally novel siderophore from Rhizobium meliloti. *J Am Chem Soc* 107: 1739–1743.
20. Kügler S, Cooper RE, Boessneck J, Küsel K, Wichard T. 2020. Rhizobactin B is the preferred siderophore by a novel *Pseudomonas* isolate to obtain iron from dissolved organic matter in peatlands. *Biometals* 33: 415–433.
21. Challis GL. 2005. A widely distributed bacterial pathway for siderophore biosynthesis independent of nonribosomal peptide synthetases. *Chem biochem* 6: 601-611.

22. Oves-Costales D, Kadia N, Challis GL. 2009. The long-overlooked enzymology of a nonribosomal peptide synthetase-independent pathway for virulence-conferring siderophore biosynthesis. *Chem Commun* 43: 6530-6541.
23. Persmark M, Pittman P, Buyer JS, Schwyn B, Gill Jr PR, Neilands JB. 1993. Isolation and structure of rhizobactin 1021, a siderophore from the alfalfa symbiont *Rhizobium meliloti* 1021. *J Am Chem Soc* 115: 3950–3956.
24. Budzikiewicz H. 1997. Siderophores of fluorescent pseudomonads. *Z Naturforsch C J Biosci* 52: 713–720.
25. Barry SM, Challis GL. 2009. Recent advances in siderophore biosynthesis. *Curr Opin Chem Biol* 13: 205-215.
26. Bindereif A, Neilands JB. 1983. Cloning of the aerobactin mediated iron assimilation system of plasmid ColV. *J Bacteriol* 153: 1111–1113.
27. De Lorenzo V, Bindereif A, Paw BH, Neilands JB. 1986. Aerobactin biosynthesis and transport genes of plasmid colV-K30 in *Escherichia coli* K-12. *J Bacteriol* 165: 570–578.
28. Ramakrishnan G, Pérez NM, Carroll C, Moore MM, Nakamoto RK, Fox TE. 2019. Citryl Ornithine Is an Intermediate in a Three-Step Biosynthetic Pathway for Rhizoferrin in *Francisella*. *ACS Chem Biol* 14: 1760-1766.
29. Cotton JL, Tao J, Balibar CJ. 2009. Identification and characterization of the *Staphylococcus aureus* gene cluster coding for staphyloferrin A. *Biochemistry* 48: 1025-1035.
30. Dehner CA, Barton L, Maurice PA, DuBois JL. 2011. Size-dependent bioavailability of hematite (α-Fe2O3) nanoparticles to a common aerobic bacterium. *Environ Sci Technol* 45 : 977-983.

31. Mridha S, Kümmerli R. 2022. Coordination of siderophore gene expression among clonal cells of the bacterium *Pseudomonas aeruginosa*. *Commun Biol* 5: 545.
32. Dave BP, Dubc HC. 2000. Regulation of siderophore production by iron Fe(III) in certain fungi and fluorescent pseudomonads. *Indian J Exp Biol* 38: 297–299.
33. Van Den Berghe M, Merino N, Nealson KH, West AJ. 2021. Silicate minerals as a direct source of limiting nutrients: Siderophore synthesis and uptake promote ferric iron bioavailability from olivine and microbial growth. *Geobiolog* 19: 618-630.
34. Akafia MM, Harrington JM, Bargar JR, and Duckworth OW. (2014). Metal oxyhydroxide dissolution as promoted by structurally diverse siderophores and oxalate. *Geochim Cosmochim Acta* 141: 258–269.
35. Duckworth OW, Akafia MM, Andrews MY, Bargar JR. 2014. Siderophore-promoted dissolution of chromium from hydroxide minerals. *Environ Sci Process Impacts* 16: 1348-1359.
36. Carroll CS, Grieve CL, Murugathasan I, Bennet AJ, Czekster CM, Liu H, Naismith J, Moore MM. 2017. The rhizoferrin biosynthetic gene in the fungal pathogen *Rhizopus delemar* is a novel member of the NIS gene family. *Int J Biochem Cell Biol* 89: 136-146.
37. Sullivan JT, Jeffery EF, Shannon JD, Ramakrishnan G. 2006. Characterization of the siderophore of *Francisella tularensis* and role of *fslA* in siderophore production. *J Bacteriol* 780: 3785-3795.
38. Schalk IJ, Rigouin C, Godet J. 2020. An overview of siderophore biosynthesis among fluorescent Pseudomonads and new insights into their complex cellular organization. *Environ microbiol* 22: 1447-1466.
39. Mathew A, Eberl L, Carlier AL. 2014. A novel siderophore-independent strategy of iron uptake in the genus *Burkholderia. Mol microbiol* 91: 805-820.

40. Min L, Guo L, Ye J. 2019. Mechanism of *Burkholderia pyrrocinia* JK-SH007 growth-promoting to plant via siderophore-mediation. *Journ Nanjing Forest Univ Nat Sci Ed* 43: 165-172.
41. Alice AF, Lopez CS, Lowe CA, Ledesma MA, Crosa JH. 2006. Genetic and transcriptional analysis of the siderophore malleobactin biosynthesis and transport genes in the human pathogen *Burkholderia pseudomallei* K96243. *J Bacteriol* 188: 1551–1566.
42. Calvaruso C, Turpault MP, Frey-Klett P. 2006. Root-associated bacteria contribute to mineral weathering and to mineral nutrition in trees: a budgeting analysis. *Appl Environ Microbiol* 72: 1258-1266.
43. Koele N, Turpault MP, Hildebrand EE, Uroz S, Frey-Klett P. 2009. Interactions between mycorrhizal fungi and mycorrhizosphere bacteria during mineral weathering: budget analysis and bacterial quantification. *Soil Biol and Biochem* 41: 1935-1942.
44. Calvaruso C, Turpault MP, Leclerc E, Frey-Klett P. 2007. Impact of ectomycorrhizosphere on the functional diversity of soil bacterial and fungal communities from a forest stand in relation to nutrient mobilization processes. *Microb Ecol* 54: 567–577.
45. Chilton MD, Currier TC, Farrand SK, Bendich AJ, Gordon MP, Nester EW. 1974. *Agrobacterium tumefaciens* DNA and PS8 bacteriophage DNA not detected in crown gall tumors. *Proc Natl Acad Sci* 71: 3672–3676.
46. Pospiech A, Neumann B. 1995. A versatile quick-prep of genomic DNA from gram-positive bacteria. *Trends in genetics: TIG*, 11 : 217-218.
47. Schwyn B, Neilands JB. 1987. Universal chemical assay for the detection and determination of siderophores. *Anal Biochem* 160: 47–56.

48. Dixon JB, Weed SB, Dinauer RC. (eds) 1989. Minerals in soil environments, 2nd ed. Madison, WI, USA: Soil Science Society of America.
49. Picard L, Turpault MP, Oger P, Uroz S. 2021. Identification of a novel type of glucose dehydrogenase involved in the mineral weathering ability of *Collimonas pratensis* strain PMB3(1). *FEMS Microbiol Ecol* 97: fiaa232.
50. Vallenet D, Calteau A, Dubois M, Amours P, Bazin A, *et al*. 2019. MicroScope: an integrated platform for the annotation and exploration of microbial gene functions through genomic, pangenomic and metabolic comparative analysis. *Nucleic Acids Res* 4: D579–D589.
51. Blin K, Shaw S, Kloosterman AM, Charlop-Powers Z, van Weezel GP, Medema MH, Weber T. 2021. antiSMASH 6.0: improving cluster detection and comparison capabilities. *Nucleic Acids Res* 2: 29-35.
52. Altschul SF, Gish W, Miller W, Myers EW, Lipman DJ. 1990. Basic local alignment search tool. *J Mol Biol* 215: 403-410.
53. Gouy M, Guindon S, Gascuel O. 2010. SeaView version 4: a multiplatform graphical user interface for sequence alignment and phylogenetic tree building. *Mol Biol Evol* 27: 221-224.
54. R Core Team (2021). R: A language and environment for statistical computing. R Foundation for Statistical Computing, Vienna, Austria. URL

803 **Figure Legends.**

804

805 **Figure 1. Growth assay.** The growth of the WT strain (**A**) and *rhiE*::Gm mutant (**B**) was
806 monitored in presence of different iron concentrations (*i.e.,* 0, 0.5, 1, 5, 10 $mg.L^{-1}$ of Fe) in AB
807 medium depleted of iron. The growth was studied under orbital shaking at 25 ºC for 90 h. The
808 absorbance was measured at 600 nm every 3 hours. Each dot is the mean of independent
809 triplicates.

810

811 **Figure 2. Impact of increasing concentrations of iron on the chelating activity of the WT**
812 **and mutant (***rhiE*::Gm**) strains.** To determine the concentration of iron inhibiting
813 siderophore production, liquid cultures of WT (red) and *rhiE*::Gm (blue) strains were
814 performed with different concentrations of iron (*i.e.,* 0, 0.1, 0.2, 0.3, 0.4, 0.5, 0.6, 0.7, 0.8, 0.9,
815 1, 1.5, 2, 2.5, 5 $mg.L^{-1}$). Pure water (grey) was used as a negative control. After 3 days, the
816 absorbance at 655 nm was measured. The decrease of the measured absorbance means the
817 presence of chelating molecules since the media coloration changes from blue to yellow and
818 the absorbance measured at 655 nm measures blue color intensity.

819

820 **Figure 3. Hematite weathering potential of strain PML1(12) and its** *rhiE*::Gm **mutant.**
821 The weathering ability was evaluated by the measure of iron released from hematite in ABm
822 medium devoid of iron, after 7 days of incubation at 25 °C under agitation (200 rpm). (**A**)
823 **Concentration of iron released in solution**. The iron released from hematite was measured
824 by ferrospectral determination (optical density measured at 595_{nm}). Abbreviations were used
825 as follows: WT + H, wild type strain plus hematite; WT, wild type strain; *rhiE*::Gm + H,
826 mutant strain plus hematite; *rhiE*::Gm, mutant strain; abiotic + h, non-inoculated condition
827 plus hematite; abiotic, non-inoculated condition. Non-inoculated conditions (abiotic control

with and without hematite) were used as controls. Samples with the same letter indicate no significant difference ($P<0.05$). **(B) Siderophore activity**. The siderophore activity of the different samples was determined using the CAS method. The yellow color indicates siderophore activity. For each measure, the results are the mean of independent triplicates.

Figure 4. **HPLC analysis and UV detection.** The pre-purified supernatant of the WT strain (red), *rhiE*::Gm mutant (blue) and non-inoculated medium (grey) were monitored at 210 nm after HPLC separation using a Milli-Q water / acetonitrile + 0.2% TFA gradient for 25 min at 1 $mL.min^{-1}$. To determine the presence of siderophore activity, fractions were collected during the HPLC run and tested using the liquid CAS assay. Positive fractions for siderophore presence are highlighted with black arrows. **(A)** A major peak (peak 1) at retention time of 0.84 min was identified. **(B)** A second peak (peak 2) of lower intensity, with a retention time of 3.88 min , was identified after CAS test.

Figure 5. Identification, fragmentation profile and chemical structure of rhizobactin. (A) Mass spectrum of HPLC positive fractions showing the parent ion of the putative chelating molecule at m/z=378.1868 (raw formula: $C_{15}H_{25}O_8N_3$). **(B)** Fragmentation pattern of the chelating molecule seen at m/z=378.1868, revealing a perfect agreement with previous experimental MS^2 results done on the rhizobactin identified in *Sinorhizobium meliloti* DM4 by Smith *et al.* (1985) and in *Pseudomonas sp*. FEN by Kügler *et al.* (2020). The major product ions are: 289.1351 (in blue, consecutive to alanine loss), 200.0882 (in yellow, formed as a result of loss of ethylenediamine and alanine and an additional carboxylic group), 116.0681 (in red, corresponding to malic acid ion - H_2O) and 84.0790 (in green, corresponding to decarboxylated lysine ion) **(C)** Chemical structure (according to Smith *et al.,* 1985) and fragmentation pattern of the rhizobactin. Same colors as in panel A are used to

highlight the correspondence of the chemical moieties of rhizobactin and product ions. Dotted boxes are used to highlight lost ions while undotted boxes mark the remaining structure of the molecule.

Figure 6. Isotopic pattern of iron complexes. Comparison between **(A)** the experimentally observed isotopic pattern of the putative iron(III) siderophore complex ion (m/z=431.0963), and **(B)** the theoretical isotopic profile of the complex $[(C_{15}H_{25}O_8N_3\text{-}2H)+Fe^{III}]^+$, $C_{15}H_{25}O_8N_3$ being the raw formula associated with the putative siderophore of m/z=378.1868.

Figure 7. Organization of the cluster of genes involved in rhizobactin biosynthesis in different strains. Each arrow represents one gene, and its size was scaled according to gene length. Gene annotation is shown in the right and the complete description is provided in Table 1. Light grey, dark grey and green genes are involved in siderophore transport. In blue, red, and yellow, genes are involved in siderophore biosynthesis. In black, genes involved with siderophore production regulation. In bold, strains for which rhizobactin synthesis was demonstrated.

Figure 8. Neighbor-joining phylogenetic analysis of NIS synthetases. A total of 24 experimentally validated and two proposed NIS-synthetases were aligned using MUSCLE algorithm and the phylogenetic tree was constructed using SeaView. The code between brackets corresponds with the NCBI accession number for each protein sequence. NIS-synthetases are colored depending on their specificity of substrate and thus their group: A (pink), A' (red), B (green), C (blue), C' (yellow). The enzymes presented in this study (*i.e.,* RhiE and putative rhizobactin synthetases) are shown in black.

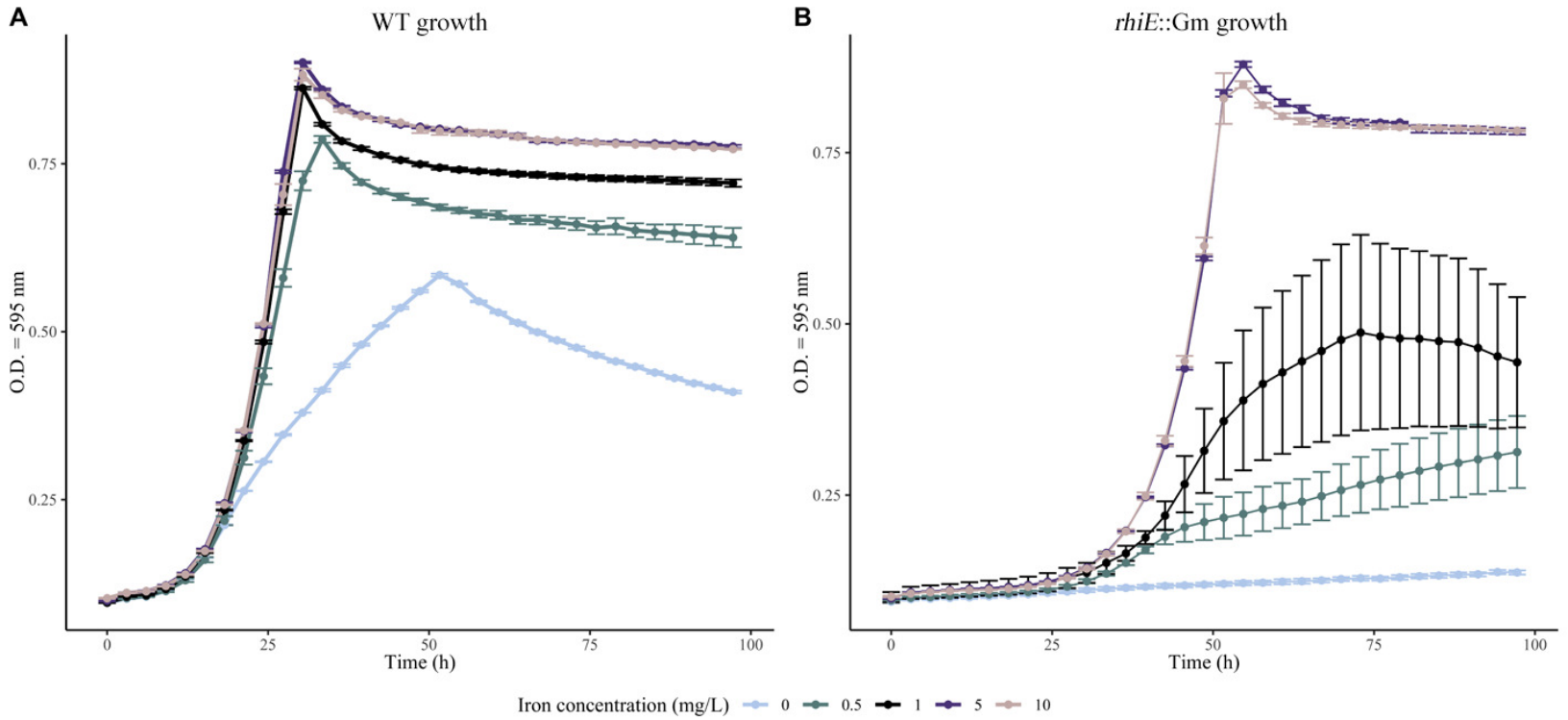
A
WT growth
B
rhiE::Gm growth
O.D. = 595 nm
0.25
0.50
0.75
0
25
50
75
100
Time (h)
Iron concentration (mg/L)
0
0.5
1
5
10

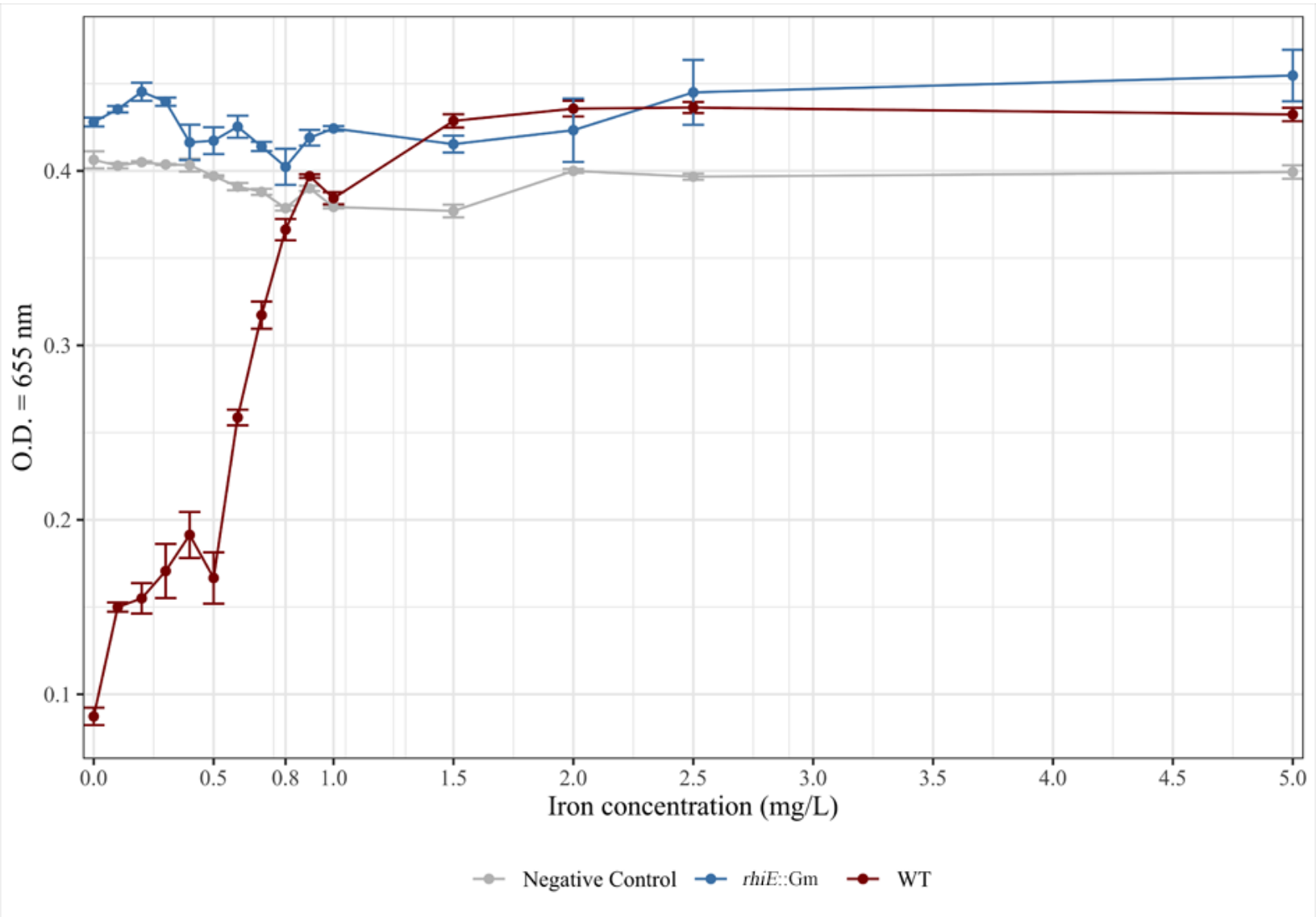
O.D. = 655 nm
0.1
0.2
0.3
0.4
0.0
0.5
0.8
1.0
1.5
2.0
2.5
3.0
3.5
4.0
4.5
5.0
Iron concentration (mg/L)
Negative Control
rhiE::Gm
WT

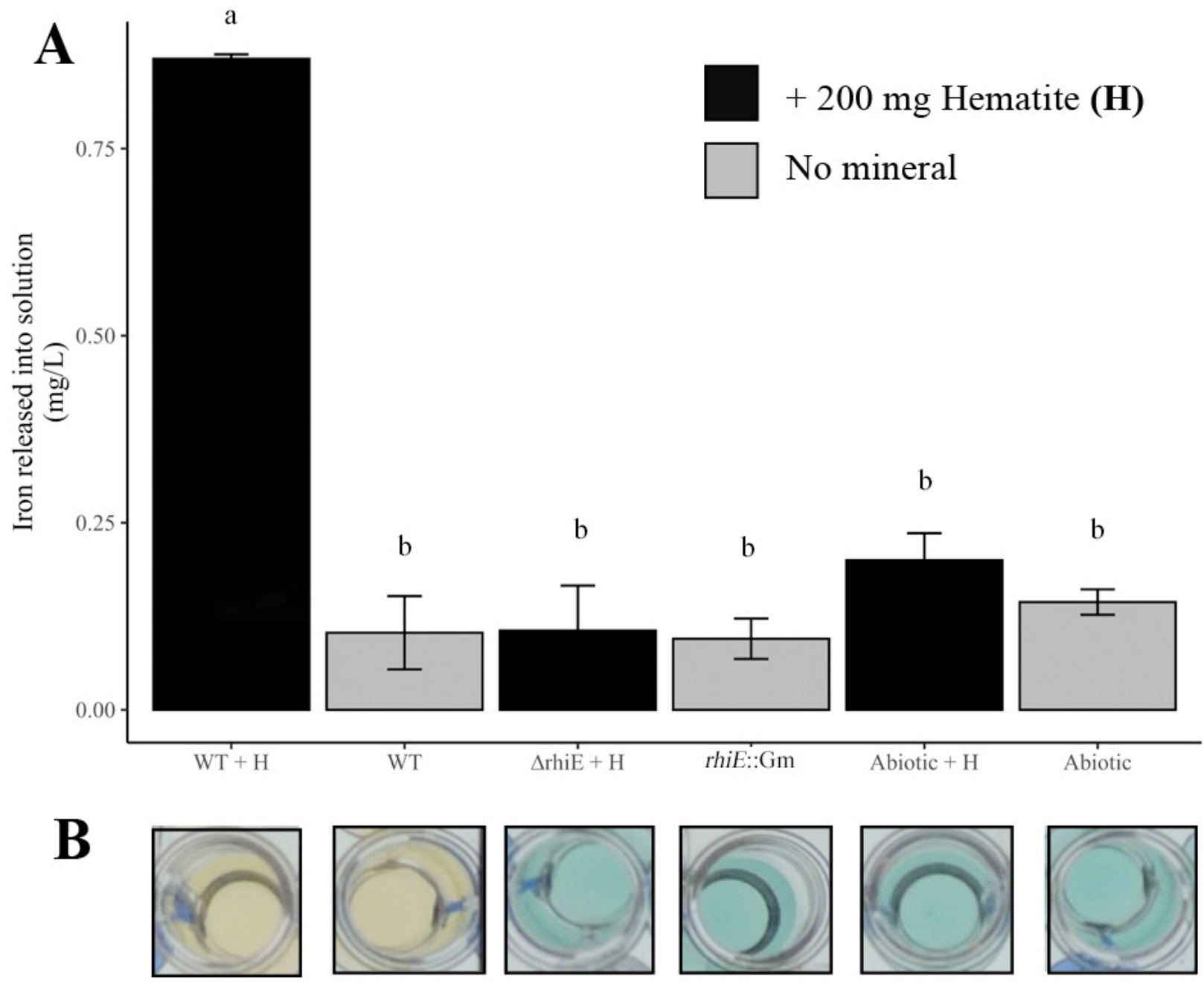
A
a
b
b
b
b
b
+ 200 mg Hematite (H)
No mineral
Iron released into solution (mg/L)
0.00
0.25
0.50
0.75
WT + H
WT
ΔrhiE + H
rhiE::Gm
Abiotic + H
Abiotic
B

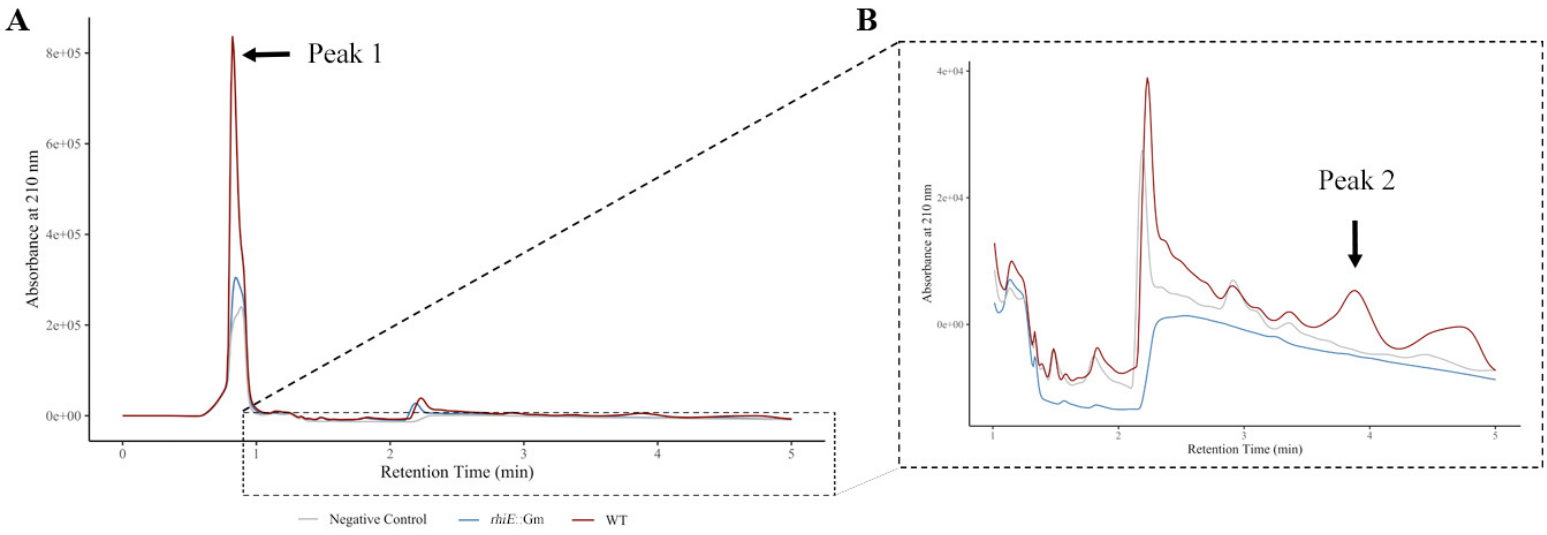
A
B
Peak 1
Peak 2
Absorbance at 210 nm
Retention Time (min)
8e+05
6e+05
4e+05
2e+05
0e+00
4e+04
2e+04
0
1
2
3
4
5
Negative Control
rhiE::Gm
WT

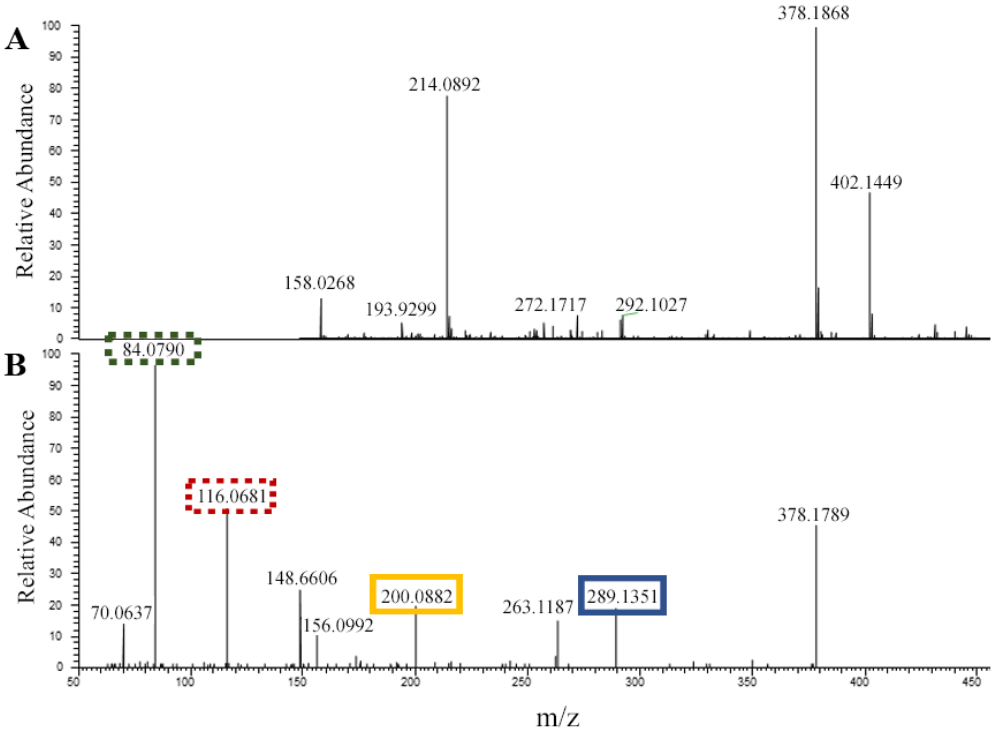
A
Relative Abundance
378.1868
214.0892
402.1449
158.0268
193.9299
272.1717
292.1027
B
Relative Abundance
84.0790
116.0681
378.1789
148.6606
200.0882
263.1187
289.1351
70.0637
156.0992
m/z

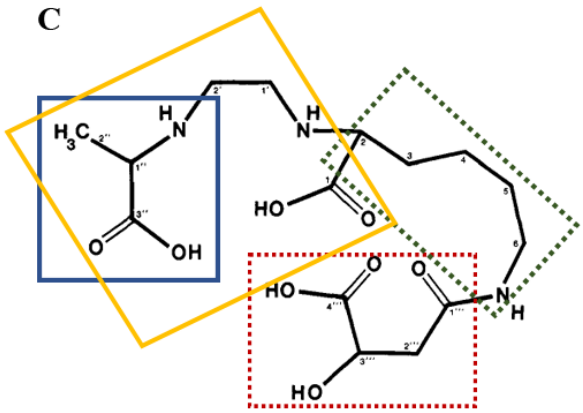
C
H3C
H
N
HO
O
OH
HO
O
O
N
H
HO

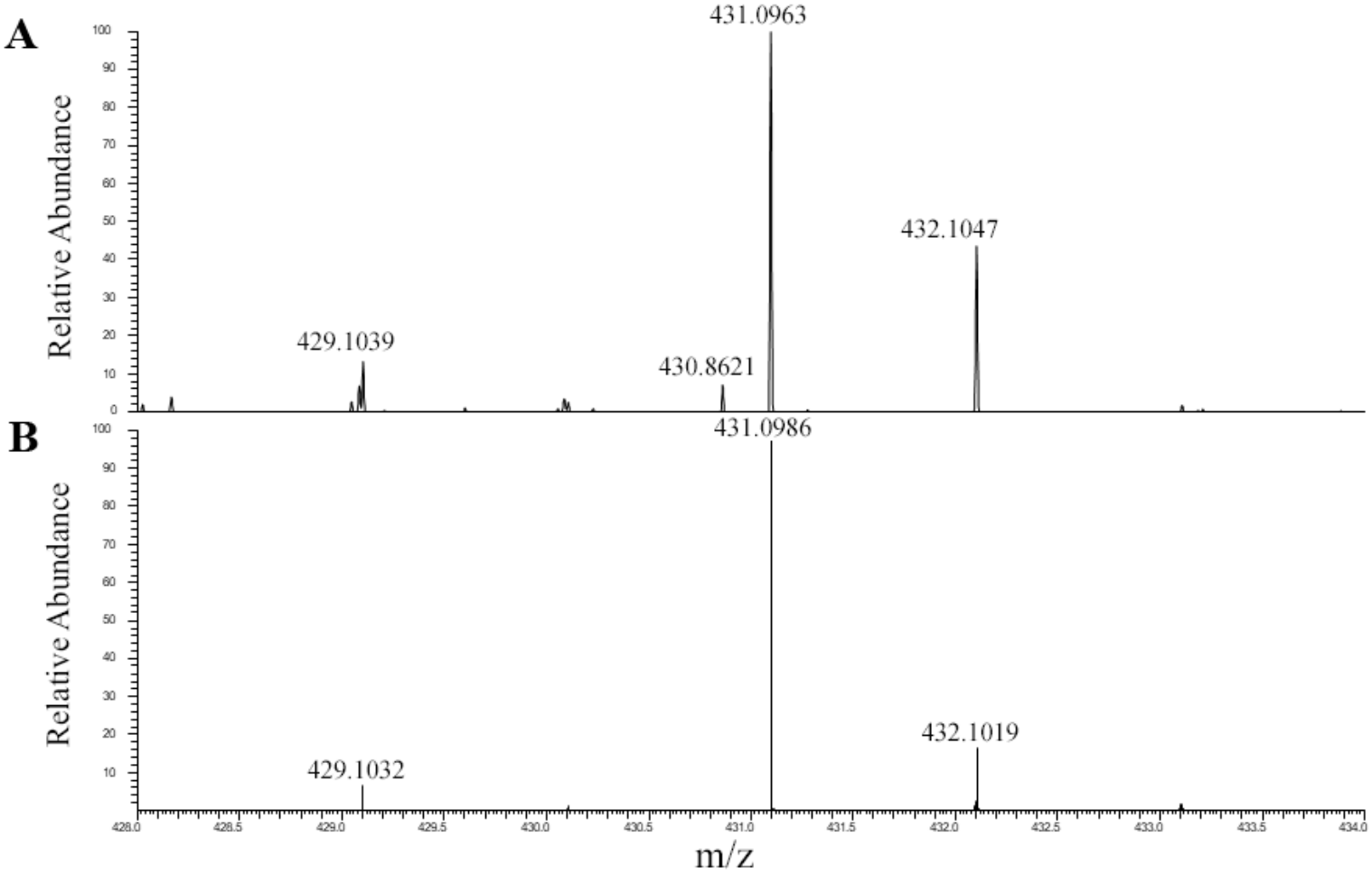
A
431.0963
432.1047
429.1039
430.8621
Relative Abundance
B
431.0986
432.1019
429.1032
Relative Abundance
m/z

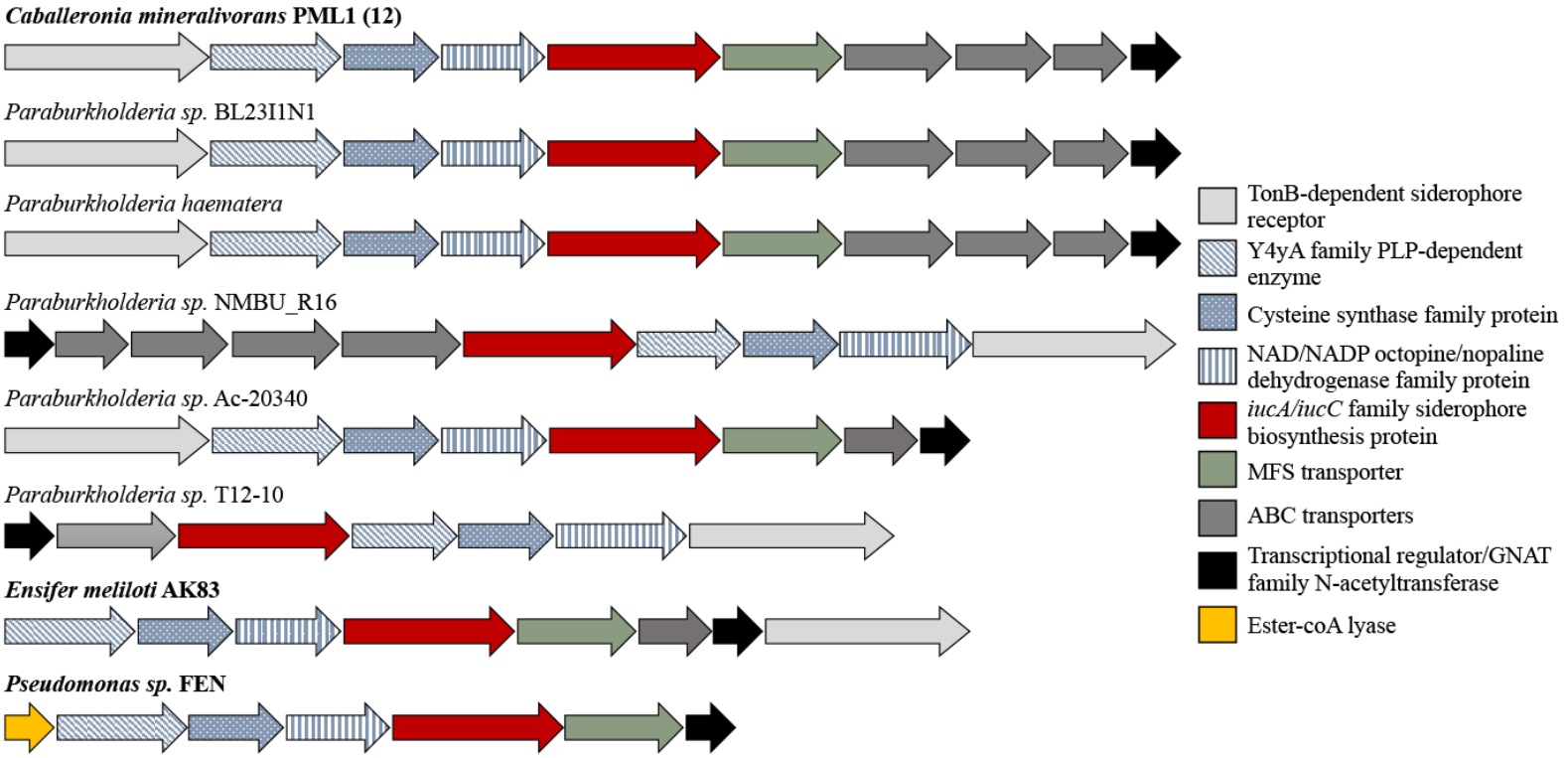
Caballeronia mineralivorans **PML1 (12)**
Paraburkholderia sp. BL23I1N1
Paraburkholderia haematera
Paraburkholderia sp. NMBU_R16
Paraburkholderia sp. Ac-20340
Paraburkholderia sp. T12-10
***Ensifer meliloti* AK83**
***Pseudomonas sp.* FEN**
TonB-dependent siderophore receptor
Y4yA family PLP-dependent enzyme
Cysteine synthase family protein
NAD/NADP octopine/nopaline dehydrogenase family protein
iucA/iucC family siderophore biosynthesis protein
MFS transporter
ABC transporters
Transcriptional regulator/GNAT family N-acetyltransferase
Ester-coA lyase

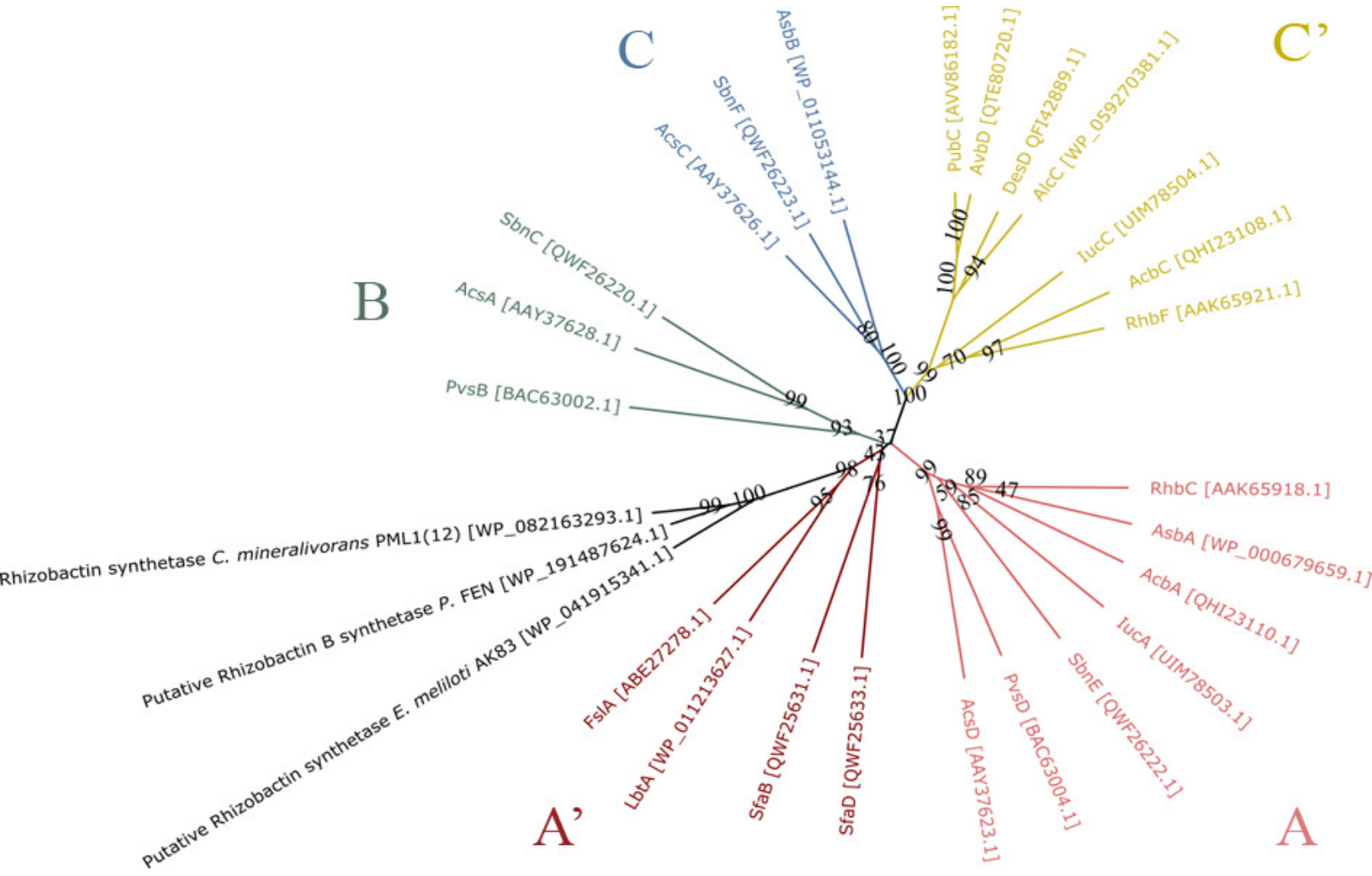
C
C'
B
A'
A
AsbB [WP_011053144.1]
SbnF [QWF26223.1]
AcsC [AAY37626.1]
SbnC [QWF26220.1]
AcsA [AAY37628.1]
PvsB [BAC63002.1]
PubC [AVV86182.1]
AvbD [QTE80720.1]
DesD QFI42889.1]
AlcC [WP_059270381.1]
IucC [UIM78504.1]
AcbC [QHI23108.1]
RhbF [AAK65921.1]
RhbC [AAK65918.1]
AsbA [WP_000679659.1]
AcbA [QHI23110.1]
IucA [UIM78503.1]
SbnE [QWF26222.1]
PvsD [BAC63004.1]
AcsD [AAY37623.1]
SfaD [QWF25633.1]
SfaB [QWF25631.1]
LbtA [WP_011213627.1]
FslA [ABE27278.1]
Putative Rhizobactin synthetase E. meliloti AK83 [WP_041915341.1]
Putative Rhizobactin B synthetase P. FEN [WP_191487624.1]
Rhizobactin synthetase C. mineralivorans PML1(12) [WP_082163293.1]

Table 1. **Description of the NRPS-independent gene region involved in siderophore production by *Caballeronia mineralivorans* strain PML1(12).** Each gene product of the cluster is presented by its NCBI accession number. The annotation is based on BLASTp homology. NIS synthetases showing the highest homology with RhiE of strain PML1(12) are shown.

Putative function	Accession number (NCBI)	Length	Gene	Annotation (based in BLASTp Homology)	Homology
Transport	KLU26370.1	745	*rhiA*	TonB-dependent siderophore receptor	88.19% *Paraburkholderia sp.* BL23IN1 (WP_120293907.1)
Synthesis	KLU26369.1	480	*rhiB*	Y4yA family PLP-dependent enzyme	80.62% *Paraburkholderia haematera* (CAE6738131.1)
Synthesis	KLU26368.1	346	*rhiC*	Cysteine synthase family protein	93.64% *Paraburkholderia sp*. BL23IN1 (WP_120293908.1)
Synthesis	KLU26367.1	388	*rhiD*	NAD/NADP octopine/nopaline dehydrogenase family protein	87.37% *Paraburkholderia haematera* (WP_236066808.1)
Synthesis	KLU26366.1	635	*rhiE*	*iucA/iucC* family siderophore biosynthesis protein	85.83% *Paraburkholderia sp.* BL23IN1 (WP_120293909.1)
Transport	KLU26365.1	421	*rhiF*	MFS transporter	85.34% *Paraburkholderia haematera* (WP_211611243.1) *Paraburkholderia sp*. BL23IN1 (WP_120293910.1)
Transport	KLU26364.1	398	*rhiG*	ABC transporter substrate-binding protein	88.69% *Paraburkholderia haematera* WP_211611244.1
Transport	KLU26363.1	353	*rhiH*	Iron ABC transporter permease	92.63% *Paraburkholderia sp.* BL23IN1 WP_120293912.1
Transport	KLU26362.1	265	*rhiI*	ABC transporter ATP-binding protein	92.83% *Paraburkholderia* sp. BL23IN1

					WP_120293913.1
Regulation	KLU26361.1	138	*rhiJ*	Transcriptional regulator/GNAT family N-acetyltransferase	87.71% *Caballeronia sordidicola* WP_031357714

Table 2. List of bacterial strains, constructions and primers used in this study.

Strains, plasmids, or primers	Characteristics	Reference
Strains		
Caballeronia mineralivorans		
Strain PML1(12)	Wild type strain	[18]
rhiE::Gm (PML1(12)(*rhiE*::Gm))	Wild type strain, with Gm^R cassette inserted in double crossing over	This study
Escherichia coli		
DH5α	*supE44*, Δ*lacU169*, (Φ*lac*ZΔM15), *recA1, endA1*, *hsdR17*, *thi-1, gyrA96*, *relA1*	Lab collection
S17.1λpir	Tpr Sm^R *recA*, *thi, pro*, *hsdRM*$^+$, RP4::2-Tc::Mu::Km Tn7 λpir	Lab collection
Plasmids		
pUC1318	Amp^R, Gm^R	Lab collection
pGEM-T Easy	Amp^R	Kit Promega
pGEM-*rhiE*_SmaI	pGEM-T Easy carrying a *rhiE* gene	This study
pGEM-*rhiE*::Gm	pGEM-*rhiE*::Gm with insertion in *Sma*I of the Gm^R cassette	This study
pK19mob	Km^R	Lab collection
pK19mob-*rhiE*::Gm	pK19mob containing a *Eco*RI fragment obtained from pGEM-*rhiE*::Gm	This study
Primers (Tm = 54 °C)		
For_*rhiE*	5'- ATGAAGACCACTCCTTCGCTATT - 3'	This study
Rev_*rhiE_Sma*I	5'- GCACCGGTCCCGGGAGCCGCGGCAT - 3'	This study
For_*rhiE_Sma*I	5'- ATGCCGCGGCTCCCGGGACCGGTGC - 3'	This study
Rev_*rhiE*	5'- TCAACCCTCGTTGTGCGCCGCCAGC - 3'	This study

Gm^R, Km^R, Sm^R, and Amp^R, indicate gentamicin, kanamycin, spectinomycin and ampicillin resistance cassettes, respectively.